This article has been accepted for publication in a future issue of this journal, but has not been fully edited. Content may change prior to final publication. Citation information: DOI 10.1109/TPWRD.2015.2443560, IEEE Transactions on Power Delivery



# Enhanced Analytical Method for the Calculation of the Maximum Inrush Currents of Single-Phase Power Transformers

Saeed Jazebi, *Member, IEEE*, Francisco de León, *Fellow, IEEE*, Nicholas Wu

***Abstract*—In this paper an accurate analytical method is proposed to compute the maximum inrush currents for single-phase transformers. The worst case scenarios for inrush currents caused by switching at the voltage zero crossing with the highest possible residual flux are investigated. Hysteresis is modeled with piece-wise linear approximations. Hence, it is assumed that the transformer is always operating on linear sections of the magnetizing curve. The maximum inrush current is computed with simple steps from the solution of the linear governing differential equations. The method is simple and thus suitable to be included in the transformer design program (or even using a calculator). Comprehensive studies are carried out to evaluate the proposed method versus laboratory measurements and EMTP simulations. Results indicate a significant improvement from published formulae in the literature. The principal advantages of the technique are its accuracy and simplicity. A step-by-step numerical example illustrates how easy it is to estimate the maximum inrush currents.**

***Index Terms*—Inrush currents, phase-hop, transformers.**

## I. Nomenclature

| | |
|---|---|
| $t$ [s] | Time |
| $\theta$ [rad] | Switching angle |
| $V_m$ [volts] | Peak of the voltage |
| $V_{rms}$ [volts] | rms voltage |
| $\omega$ [rad/s] | Angular frequency |
| $\lambda$ [Wb] | Magnetic flux linkages |
| $\lambda_0$ [Wb] | Residual flux |
| $\lambda_s$ [Wb] | Saturation flux |
| $\lambda_n$ [Wb] | Nominal magnetic flux ($V_m/\omega$) |
| $B$ [T] | Magnetic flux density |
| $B_0$ [T] | Flux density corresponding to $\lambda_0$ |
| $B_s$ [T] | Flux density corresponding to $\lambda_s$ |
| $B_n$ [T] | Flux density corresponding to $\lambda_n$ |
| $L$ [H] | Transformer magnetizing inductance |
| $L_{sc}$ [H] | Short circuit inductance of network |
| $L'_s$ [H] | Saturation inductance |
| $L_s$ [H] | $L_{sc}+L'_s$ |
| $L'_m$ [H] | Magnetizing inductance below the knee point |
| $L_m$ [H] | $L_{sc}+L'_m$ |
| $R_{sc}$ [Ω] | Short circuit resistance of the network |
| $R_T$ [Ω] | Transformer winding resistance |
| $R$ [Ω] | Total resistance ($R=R_{sc}+R_T$) |
| $A$ [m$^2$] | Cross sectional area of the flux path |
| $N$ | Number of turns |
| $T$ [s] | Power frequency period |

## II. Introduction

INRUSH currents associated with power transformer energization have the potential to produce mechanical stresses on the windings, damage insulation, generate harmonic distortion in power systems, create voltage sags, and cause malfunction of differential protection relays. Hence, it is necessary to predict the most severe inrush currents for the proper coordination of protection devices, to prevent power outages, and to avoid possible damages.

Several analytical formulae are available in the literature for the calculation of inrush currents during transformer energization [1]-[16]. Some are developed to predict this phenomenon for single-phase units [1]-[11] and some others are especially derived for three-phase transformers [12]-[16]. In all of them, assumptions are made to obtain simple-to-use formulae. For example, some references neglect the terminal resistance for simplifications [1]-[5], which is not an appropriate approximation especially for small transformers with higher resistance values or for transformers with small saturation inductance (frequently called "air-core" inductance). A small saturation inductance causes higher inrush currents and therefore the voltage drop in the winding resistances becomes significant. For higher inrush currents the difference between the terminal voltage and the internal (linking) voltage of the transformer increases. Therefore, computation of the incremental flux linkages by integration of the terminal voltage creates crucial errors. Simulation results presented in the paper show the importance of the proper calculation of the flux linkages.

Some references include the leakage inductance in the equivalent circuit for inrush current calculation [12]-[14]. However, the highest inrush currents happen when the transformer is open circuited [1]-[16]. In this condition, the current in the secondary winding is zero. Therefore, interaction between the magnetic field of the primary and the secondary winding does not exist and the leakage inductance is meaningless [17], [18]. Leakage inductance is a quantity defined for two windings and is not involved in no-load normal operation

S. Jazebi, F. de León, and N. Wu are with the Department of Electrical and Computer Engineering, NYU Polytechnic School of Engineering, Six Metrotech Center, Brooklyn, NY, 11201 (e-mails: jazebi@ieee.org, fdeleon@nyu.edu, nickwu2010@gmail.com).

This article has been accepted for publication in a future issue of this journal, but has not been fully edited. Content may change prior to final publication. Citation information: DOI 10.1109/TPWRD.2015.2443560, IEEE Transactions on Power Delivery



or transients, such as open circuit inrush current.

The worst cases for inrush currents happen when the core has residual flux and the switching occurs at the instant of voltage zero-crossing with a polarity that increases the flux linkages in the core. This paper proposes an analytical method to estimate the amplitude of these cases considering the maximum possible residual flux in the core. This is done with a step-by-step routine and the closed-form solution of the differential equations of the transformer equivalent electrical circuit. Two types of transformers are investigated: a toroidal-type transformer and a standard shell-type transformer. The worst case of inrush current (considering the initial flux) is computed and then compared versus simulations and the methods of references [9]-[11]. Reference [11] proposes the following formula for the maximum inrush currents:

$$I_{max} = \frac{V_m}{\sqrt{(\omega L_s')^2 + R^2}} \left(1 + \cos\theta + \frac{\lambda_0 - \lambda_s}{\lambda_n}\right)$$

This formula is similar to the equation presented in [9] when substituting $\lambda$=$N$×$B$×$A$ and $\theta$=0 to calculate the worst case of inrush current as a function of the magnetic flux density:

$$I_{max} = \frac{\sqrt{2}V_{rms}}{\sqrt{(\omega L_s')^2 + R^2}} \left(\frac{2B_n + B_0 - B_s}{B_n}\right)$$

and the Schwartz formula is as follows [10]:

$$I_{max} = \frac{V_m}{\omega(L_s' + L_{sc})} \left(2 + \frac{\omega(\lambda_0 - \lambda_s)}{V_m}\right)$$

The latter formula neglects the winding resistance. This assumption in some cases may result in errors especially for smaller transformers. The method of this paper estimates inrush currents for magnetized core transformers with high precision for different hysteretic shapes. The analytical calculations are supported with laboratory measurements and validated EMTP simulations. The required transformer parameters are derived from 3D finite element simulations and standard laboratory measurements.

## III. Analytical Solutions for the Worst Case Scenarios of Magnetizing Inrush Currents

There are two severe cases of inrush currents, both happen when the switching occurs at the voltage zero-crossing moment of the voltage waveform. The amplitude of inrush currents depends on the initial flux trapped in the core. The flux linkages change according to the pre-re-energization operating condition of the transformer. In the case of a transformer completely disconnected from the source, and open circuited, the current of the terminal becomes exactly zero. Therefore, the operating point on the magnetizing characteristic moves to the $\lambda$ axis (zero current and with maximum remnant flux $\lambda_{r1}$ (see Fig. 1)). Therefore, the first worst case scenario is the energization of the transformer at the moment of voltage zero crossing with initial flux of $\lambda_{r1}$, and with a polarity of the voltage in the direction that builds up the flux linkages. This case, which is called "first peak" of inrush current hereafter is very well-known among power engineers [1]-[16].

In this paper another inrush current phenomenon, which produces larger amplitudes, is also analyzed. When there is a fault on the primary side, the transformer is not disconnected from the source. This situation can be modeled with a short circuit on the primary. As the result, the terminal current will not suddenly reach zero and will keep circuiting in the primary winding. Therefore, magnetic flux will be trapped in the core for a period of time depending on the total resistance and inductance of the system. The operating point in some cases may stay on the saturated section of the magnetizing curve, such as $\lambda_{r2}$ (in Fig. 1). This residual flux is higher than $\lambda_{r1}$ and as a result the transformer draws larger inrush currents after fault clearance or re-energization. This condition is valid for the single-phase transformers studied in this paper. For three phase units or for units connected to inductive/capacitive loads, the secondary voltage impacts the core flux linkages. Nevertheless, the worst case happens when the magnetic flux is trapped in the magnetic core. Although this condition is known by power engineers, it has not received the attention it deserves. Recently a few studies have been carried out to understand the phenomenon at the moment of voltage recovery after sags or interruptions [19]-[23]. A comprehensive study on this phenomenon and its other possible causes is presented in [24]; the word "*phase-hop*" was coined for this situation.

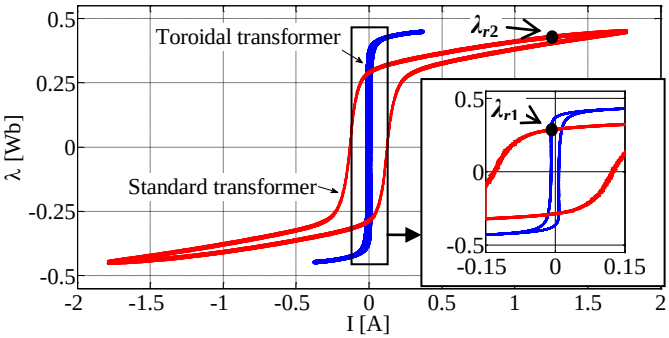


Fig. 1. Hysteresis cycle of shell-type- and toroidal-core 1 kVA transformers, and the highest possible cases of residual flux.

In conclusion, the worst case scenarios are switchings at the instant of voltage zero-crossing with a polarity that increases the flux linkages in the core. In the case of transformer with positive residual flux as shown in Fig. 1 zero crossing on the transition between negative to positive polarity leads to maximum flux linkages.

### A. First Peak of Inrush Currents

This subsection investigates the highest possible peak of inrush currents. The test setup is depicted in Fig. 2:

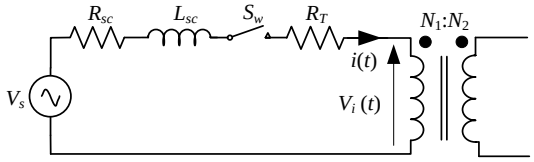


Fig. 2. Equivalent circuit of the system in the open circuit condition.

According to the principle of duality, the iron core transformer in low frequencies can be represented with a hysteretic

This article has been accepted for publication in a future issue of this journal, but has not been fully edited. Content may change prior to final publication. Citation information: DOI 10.1109/TPWRD.2015.2443560, IEEE Transactions on Power Delivery



inductor in parallel with a linear resistor [25]. The resistor has a substantially high resistance that represents the iron losses. Validated EMTP simulations demonstrated that this resistor does not affect the inrush currents significantly and could be neglected [11]. The behavior of the iron core is hysteretic. In this paper, this characteristic is linearized for different transformer operation regions. Accordingly, the calculation of inrush current is carried out in sequential steps. In each step, the nonlinearities are estimated with linear approximations. Note that the current, the voltage and the flux linkages vary with time. These parameters calculated at the end of each step are used as the initial conditions for the next step. The steps are numbered consecutively to clearly describe the computational procedure.

Fig. 3 presents the terminal current, terminal voltage, internal voltage ($V_i$), and the flux linkages during the inrush current and the phase-hop conditions. One can observe that phase-hop happens after two consecutive peaks of voltage. This phenomenon and its causes are explained in the next section. The equivalent electrical circuits of the system during the first and the second peaks of inrush currents are presented in Fig. 4(a) and Fig. 4(b), respectively.

The first peak of inrush current is computed in two steps. The first step starts at $t$=0 and ends with point (1) indicated in Fig. 3. The starting point of the second step is point (1) and the ending point is (2).

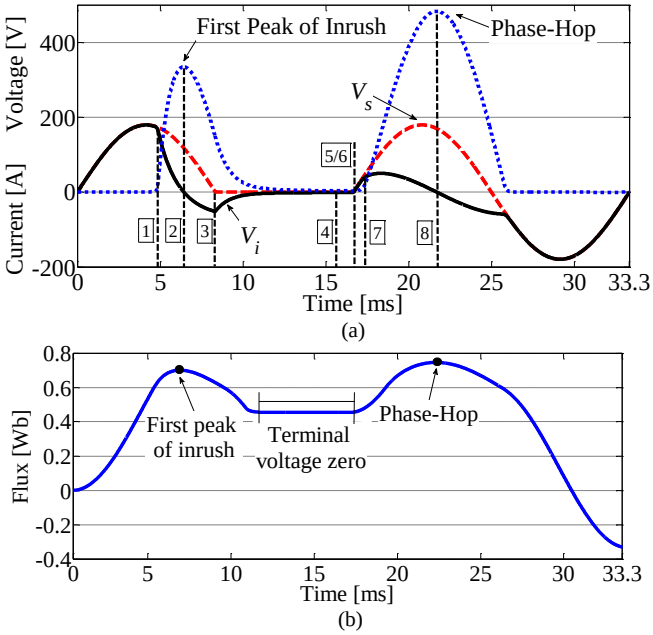


Fig. 3. Two consecutive transients; (a) inrush and phase-hop currents, voltage of the source, and voltage of the magnetizing branch ($V_i$), (b) Magnetic flux linkages.

*1) Step 1:*

After the switch is closed at $t$=0 (see Fig. 2), the electrical circuit can be represented by Fig. 4(a). Note that, $L$ represents the total inductance of the system (transformer hysteretic inductance plus the system $L_{sc}$). The hysteretic inductance is approximated with two slopes $L'_m$ below the knee point (normal operating region), and $L'_s$ for the saturation region. Note that, the IEC definition to identify the knee point is used, which is defined as the intersection of the two lines (the non-saturated and saturated lines of the exciting curve) [26]. Parameter $L'_m$ is measured with the standard open circuit test [27], and $L'_s$ the saturation inductance, can be measured with a non-ideal rectifier source [28]. Finally the two-slope inductor presented in Fig. 5 is obtained as $L_m$=$L_{sc}$+$L'_m$ and $L_s$=$L_{sc}$+$L'_s$. The error due to this approximation may be reduced using more slopes. However, comprehensive EMTP simulation studies show that a two-slope magnetizing branch is able to predict the inrush currents with acceptable engineering accuracy (of about 5%) [29]. This can be also concluded from the calculation results presented in the next sections.

The following differential equation can be written for the circuit of Fig. 4(a):

$$v_s(t) = L\frac{di}{dt} + R\, i(t) \tag{1}$$

where $V_s$=$V_m$ sin($\omega t$+$\theta$). The solution of (1) is:

$$i(t) = \frac{V_m(R\sin(\omega t) - \omega L\cos(\omega t))}{(R^2+(\omega L)^2)} + \left(i(t_i) - \frac{V_m(R\sin(\omega t_i) - \omega L\cos(\omega t_i))}{(R^2+(\omega L)^2)}\right)e^{-\frac{R(t-t_i)}{L}} \tag{2}$$

where $\theta$ = 0° to calculate the largest inrush currents. Equation (2) is used several times in the paper for the different operating regions. The proper initial conditions need to be selected for each region. In this equation, $t_i$ is the initial time and $i(t_i)$ is the corresponding initial current in each step.

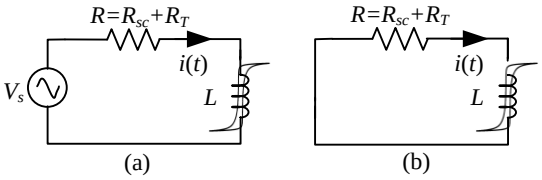


Fig. 4. Simplified circuits of Fig. 2 for various instants of inrush current.

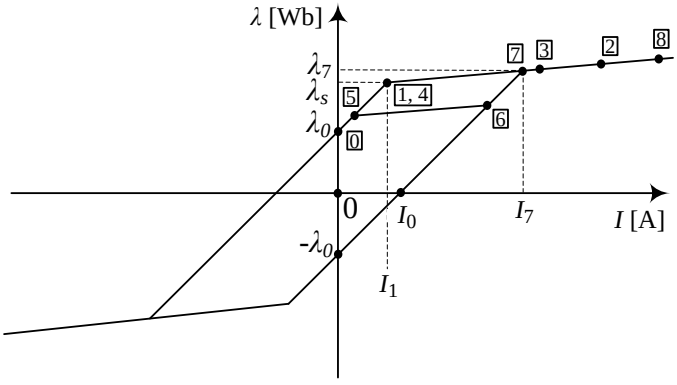


Fig. 5. Hysteretic inductance of the system represented with piecewise linear approximations by two constant slopes. The numbers correspond to different instants (see Fig. 3).

The maximum inrush current happens when the initial flux is at the maximum level and the transformer is energized at voltage zero crossing with voltage polarity that builds up the

This article has been accepted for publication in a future issue of this journal, but has not been fully edited. Content may change prior to final publication. Citation information: DOI 10.1109/TPWRD.2015.2443560, IEEE Transactions on Power Delivery



flux linkages. It is assumed that the transformer is disconnected from the source before energization. Thus, at instant $t$=0, current is zero and initial flux is at its positive maximum $\lambda_0$= $\lambda_{r1}$ (see Figs. 1 and 5). The voltage source is switched on at zero crossing going to positive polarity. Thus, the operating point moves up on the hysteresis curve. The slope of this line is $L_m$. The instant of saturation could be characterized with current $I_1$ at time $t_1$. Hence, parameter $t_1$ is defined for the time spent going from the origin to the saturation point. This parameter could be calculated with respect to the flux linkages $\lambda(t_1)$ at $t_1$,

$$\lambda(t_1) = \int_0^{t_1} V_i(t)\, dt + \lambda_0 \tag{3}$$

The terminal current when operating below the knee point (IEC definition) is very small in open circuit; therefore, the voltage drop over the winding resistance is neglected to simplify the equations. This can be concluded from Fig. 3 where the terminal and internal voltages are superimposed,

$$\lambda(t_1) \approx \int_0^{t_1} V_s(t)\ \ dt + \lambda_0 \tag{4}$$

From Fig. 5, $\lambda(t_1)$= $\lambda_s$, hence, the solution of (4) gives:

$$\frac{V_m}{\omega}[\cos(\omega t_1 + \theta)\ -\cos\theta] = \lambda_0 - \lambda_s \tag{5}$$

Considering the switching angle $\theta$ = 0° as discussed,

$$t_1 = \frac{\arccos\left[\frac{(\lambda_0 - \lambda_s)\omega}{V_m} + 1\right]}{\omega} \tag{6}$$

where $\lambda_0$ and $\lambda_s$ are extracted from the magnetizing characteristic given by the transformer manufacturer or measured in the laboratory. Finally, the current at the saturating point $i(t_1)$ is calculated by substituting $t$=$t_1$ and $L$=$L_m$ in (2) where $t_i$ = 0, yielding:

$$i(t_1) = I_1 = \frac{V_m\left[R\sin(\omega t_1) - \omega L_m \cos(\omega t_1) + \omega L_m e^{-\frac{Rt_1}{L_m}}\right]}{R^2 + (\omega L_m)^2} \tag{7}$$

*2) Step 2:*

The peak of the inrush current corresponds to the moment where the internal voltage $V_i$ is zero (see point 2 in Fig. 3). This is so because the incremental flux rises while $V_i$ is positive. Thus, the peak time ($t_{pk}$) can be calculated by solving the following equation:

$$V_i = V_m \sin(\omega t_{pk}) - Ri(t_{pk}) = 0 \tag{8}$$

The expression for the current in this region is obtained from (2), where $t_i$=$t_1$, $L$=$L_s$, and $i(t_i)$= $I_1$=$i(t_1)$. This corresponds to the region between points 1 to 2 of Fig. 5:

$$i(t) = \frac{V_m(R\sin(\omega t) - \omega L_s\cos(\omega t))}{(R^2 + (\omega L_s)^2)} + \left(i(t_1) - \frac{V_m(R\sin(\omega t_1) - \omega L_s\cos(\omega t_1))}{(R^2 + (\omega L_s)^2)}\right) e^{-\frac{R(t-t_1)}{L_s}} \tag{9}$$

Substituting (7) into (9) and $t_{pk}$, (10) is obtained (see bottom of the page). Then, (10) is substituted into (8) giving (11), also at the bottom of the page. The solution of (11) gives $t_{pk}$. This non-linear equation can be solved with the embedded Matlab function 'solve'. However, simple linear and quadratic polynomial approximations are derived for this equation in Section IV to further simplify the calculations. To calculate the first peak of inrush current, $t_{pk}$ is then substituted into (10). Therefore, the maximum peak of the inrush current could be calculated following 4 simple steps:

1. Calculate $t_1$ from (6)
2. Calculate $I_1$ from (7)
3. Calculate $t_{pk}$ from (11) or (32)
4. Calculate $i(t_{pk})$ from (10)

### *B. Phase-Hop Currents*

The phase-hop phenomenon was first introduced in [24]. This condition is usually seen during the mal-operation of off-line UPS systems, voltage sags, interruptions, and notching of voltage [24]. The transient currents produced by phase-hop are more severe than the zero crossing inrush currents. Therefore, to protect the power transformers and other power system pieces of equipment, it is necessary to estimate the maximum value of the phase-hop current.

The worst case of phase-hop occurs when the transformer iron core has the residual flux $\lambda_0$=$\lambda_{r1}$, and the energization happens at the zero crossing instant of voltage. Suppose that the transformer is energized for half a cycle and then the source is lost for the next half cycle. In this time interval, the voltage at the source terminal is zero. If the voltage recovers at the next zero crossing, two consecutive peaks of voltage with the same polarity (as shown in Fig. 3) are imposed to the

$$i(t_{pk}) = I_1 e^{-\frac{R(t_{pk}-t_1)}{L_s}} + \frac{V_m R\left[\sin(\omega t_{pk}) - \sin(\omega t_1)e^{-\frac{R(t_{pk}-t_1)}{L_s}}\right] + V_m \omega L_s\left[\cos(\omega t_1)e^{-\frac{R(t_{pk}-t_1)}{L_s}} - \cos(\omega t_{pk})\right]}{R^2 + (\omega L_s)^2} \tag{10}$$

$$V_m\sin(\omega t_{pk}) - RI_1 e^{-\frac{R(t_{pk}-t_1)}{L_s}} - \frac{V_m R^2\left[\sin(\omega t_{pk}) - \sin(\omega t_1)e^{-\frac{R(t_{pk}-t_1)}{L_s}}\right] + V_m R\omega L_s\left[\cos(\omega t_1)e^{-\frac{R(t_{pk}-t_1)}{L_s}} - \cos(\omega t_{pk})\right]}{R^2 + (\omega L_s)^2} = 0 \tag{11}$$

This article has been accepted for publication in a future issue of this journal, but has not been fully edited. Content may change prior to final publication. Citation information: DOI 10.1109/TPWRD.2015.2443560, IEEE Transactions on Power Delivery



transformer. This raises the incremental flux to the highest possible value, and consequently the highest peak of phase-hop current occurs. The phase-hop phenomenon is shown in Fig. 3. A comprehensive study on phase-hop, its causes, and its disruptive effects is presented in [24].

The most frequent cause of the phase-hop currents are voltage sags. The common voltage sags have depths between 80-90%. This means that a negative voltage appears at the terminal for the second half cycle. The amplitude of the negative voltage (between points 3 and 5) reduces the residual flux trapped in the iron core and consequently reduces the magnitude of the phase-hop current. Hence, the worst case of phase-hop happens when there is a solid fault at the terminals of the transformer for a half cycle (sag with 100% depth); see Fig. 3.

In this subsection, an analytical solution is presented to estimate the worst case of phase-hop current. According to the above explanations, the worst case of the phase-hop current occurs half a period after the zero-crossing inrush. This means that two consecutive voltage semi-cycles with the same polarity are applied to the transformer terminals. Therefore, to compute the peak value of this phenomenon, the two first steps described in the previous section are required.

*3) Step 3:*

The voltage applied to the terminals of transformer is illustrated in Fig. 3. In the transition between points 2 and 3 of Fig. 3, $V_i$ is negative. Therefore, the flux linkages decrease in this period. The objective is to find the current and flux linkages at the end of the first half period ($I_3$, $\lambda_3$). Equation (2) is utilized to calculate $I_3$ with $t_i$=$t_1$, $i(t_i)$=$I_1$=$i(t_1)$, $L$=$L_s$, and $t$=$T$/2. The reason to substitute $t$=$T$/2 is that point 3 is located at half a period after the switching instant, thus we have:

$$I_3 = \frac{V_m\left(R\sin\left(\frac{\omega T}{2}\right) - \omega L_s \cos\left(\frac{\omega T}{2}\right)\right)}{(R^2 + (\omega L_s)^2)} + \left(\frac{V_m\left[R\sin(\omega t_1) - \omega L_m \cos(\omega t_1) + \omega L_m e^{-\frac{Rt_1}{L_m}}\right]}{R^2 + (\omega L_m)^2} - \frac{V_m(R\sin(\omega t_1) - \omega L_s\cos(\omega t_1))}{(R^2 + (\omega L_s)^2)}\right) e^{-\frac{R\left(\frac{T}{2} - t_1\right)}{L_s}} \quad (12)$$

Assuming the worst case, when the operating point is still in the region representing the high saturated core ($L_s$), the flux linkages can be calculated by:

$$\lambda_3 = \lambda_s + \Delta\lambda = \lambda_s + L_s\,(I_3 - I_1) \quad (13)$$

*4) Step 4*

Step 4, investigates the transition between points 3 and 4. The objective is to compute the time, current, and flux linkages magnitude corresponding to point 4. In this time interval, the power source is lost. Therefore, the voltage is zero. As the result, current and flux linkages continue decreasing and the operating point moves down to point 4 of Fig. 5. The equivalent circuit in this condition is depicted in Fig. 4(b). The corresponding differential equation is written as:

$$L\frac{di}{dt} + Ri(t) = 0 \quad (14)$$

The solution of (14) is as follows:

$$i(t) = Ie^{-\frac{R(t-t_i)}{L}} \quad (15)$$

In this condition, the flux linkages could be calculated by taking the integral of $Ri(t)$, where the expression for $i(t)$ is given in (15). The values calculated in step 3 are substituted in (15) as initial conditions, $I$=$I_3$ and $t_i$=$T$/2, yielding:

$$\Delta\lambda = \lambda_4 - \lambda_3 = \int_{t_3}^{t_4} Ri(t)\,dt = \int_{T/2}^{t_4} RI_3 e^{-\frac{R(t-T/2)}{L_s}}\,dt \quad (16)$$

Thus, (16) is solved for $t$ to find the time at point 4 ($t_4$):

$$t_4 = \frac{T}{2} - \frac{L_s}{R}\ln\left(1 + \frac{\lambda_4 - \lambda_3}{L_s\, I_3}\right) \quad (17)$$

where $\lambda_4$=$\lambda_s$ (see Fig. 5) and $\lambda_3$ is calculated in the previous step.

*5) Step 5:*

In step 5, the flux linkages at the end of the first period (point 5) are calculated. This is done by integrating over the term $Ri(t)$ where $i(t)$ could be substituted from (15) with parameters $I$=$I_4$=$I_1$, $t_i$=$t_4$, $L$=$L_m$, and $t$=$T$/2.

$$\Delta\lambda = \lambda_5 - \lambda_4 = \int_{t_4}^{t_5} Ri(t)dt = \int_{t_4}^{T} RI_4 e^{-\frac{R(t-t_4)}{L_m}}dt \quad (18)$$

Therefore,

$$\lambda_5 = (I_4 L_m + \lambda_0)e^{-\frac{R(T-t_4)}{L_m}} \quad (19)$$

The current at this point is calculated by interpolation using the slope of the magnetizing line under the knee point ($L_m$):

$$\Delta\lambda = \lambda_5 - \lambda_s = L_m(I_5 - I_4) \Rightarrow I_5 = \frac{\lambda_5 - \lambda_s + I_4 L_m}{L_m} \quad (20)$$

*6) Step 6:*

In step 6, the transition between point 5 and point 6 happens. Here, the transition time is neglected. Therefore, the current could be estimated by (see Fig. 5):

$$I_6 = I_5 + 2I_0 \quad (21)$$

Thus,

$$\lambda_6 = \lambda_5 + \Delta\lambda = \lambda_5 + L_s(I_6 - I_5) = \lambda_5 + 2L_s I_0 \quad (22)$$

This article has been accepted for publication in a future issue of this journal, but has not been fully edited. Content may change prior to final publication. Citation information: DOI 10.1109/TPWRD.2015.2443560, IEEE Transactions on Power Delivery



It should be noted that at point 6, the equivalent circuit changes to the one in Fig. 4(a).

*7) Step 7:*

In step 7, the current in point 7 is estimated by (see Fig. 5):

$$I_7 = I_1 + 2I_0 = I_1 + \frac{2\lambda_0}{L_m} \tag{23}$$

Knowing the current $I_7$ at saturation point 7, the corresponding flux linkages could be calculated by:

$$\lambda_7 = L_m(I_7 - I_6) + \lambda_6 = L_m(I_1 + 2I_0 - I_6) + \lambda_6 \tag{24}$$

Substituting (21) into (24) yields:

$$\lambda_7 = L_m(I_1 - I_5) + \lambda_6 \tag{25}$$

*8) Step 8:*

The last step is the transition from point 6 to 7 to 8. The operating point moves with a pattern similar to the pattern seen in the transition between points 0 to 2 of Step 1 (see Figs. 3 and 5). Therefore, the same procedure is used, but with different parameters, which means calculating $t_7$ with the following expression:

$$t_7 = \frac{\arccos\left[\frac{(\lambda_6 - \lambda_7)\omega}{V_m} + 1\right]}{\omega} \tag{26}$$

This is so because parameters $\lambda_0$ and $\lambda_s$ are substituted by $\lambda_6$ and $\lambda_7$ in (26). The peak current of phase-hop corresponds to the moment that the electromotive force through the winding is zero (see point 8 in Fig. 3). Thus, the peak time $t_{pk}$ could be calculated by solving (8). The expression for current in this region is obtained from (2), where $t_i$=$t_7$, $L$=$L_s$, and $i(t_i)$=$i(t_7)$=$I_7$. Consequently, $t_{pk}$ could be substituted in the current expression to get the maximum phase-hop current. Therefore, $t_{pk}$ and $i(t_{pk})$ are derived as (27) and (28). Equation (27) is non-linear and can be solved with the embedded Matlab function 'solve'. However, simple polynomial approximations are derived for this equation in the next section. Equation (26) can be rewritten in the form of (29) using (25), (20), (19) and (17). In summary the highest peak of the phase-hop current can be calculated in 7 steps as (the first two are the same as for the first peak of inrush currents):

1. Calculate $t_1$ from (6)
2. Calculate $I_1$ from (7)
3. Calculate $I_3$ from (12)
4. Calculate $\lambda_3$ from (13)
5. Calculate $t_7$ from (29)
6. Calculate $t_{pk}$ from (28) or (30)
7. Calculate $i(t_{pk})$ from (27)

## IV. Taylor Series Expansion of (11) and (28) for the Analytical Calculation of $T_{PK}$

The most important step to calculate the first and second peaks of inrush current described above is to accurately compute the peak time ($t_{pk}$). However, (11) and (28) are non-linear equations which require numerical iterative solvers. Exhaustive simulation studies show that the peak of the currents is near the peak of the voltage wave, at π/4 (see Fig. 3(a)). This corresponds to a quarter of the period ($T$/4). Therefore, second and third order Taylor series expansions of (11) and (28) are obtained at $t_{pk}$=$T$/4. This results in linear and quadratic polynomial equations, respectively.

The linear polynomial approximation of (11) is as follows:

$$At_{pk} + B = 0 \tag{30}$$

where $A$ and $B$ are computed from:

$$\begin{aligned} A &= K_1\,\omega\cos\left(\frac{\omega T}{4}\right) - K_3\omega\sin\left(\frac{\omega T}{4}\right) - \frac{K_2 R}{L_s}e^{-\frac{RT}{4L_s}} \\ B &= K_3\left[\frac{\omega T}{4}\sin\left(\frac{\omega T}{4}\right) + \cos\left(\frac{\omega T}{4}\right)\right] + K_2 e^{-\frac{RT}{4L_s}}\left[1 + \frac{RT}{4L_s}\right] \\ &\quad + K_1\left[\sin\left(\frac{\omega T}{4}\right) - \frac{\omega T}{4}\cos\left(\frac{\omega T}{4}\right)\right] \end{aligned} \tag{31}$$

The quadratic polynomial approximation of (11) is:

$$At_{pk}^2 + Bt_{pk} + C = 0 \tag{32}$$

where:

$$A = \frac{K_2 R^2}{2L_s^2}e^{-\frac{RT}{4L_s}} - \frac{K_3\omega^2}{2}\cos\left(\frac{\omega T}{4}\right) - \frac{K_1\omega^2}{2}\sin\left(\frac{\omega T}{4}\right)$$

$$i(t_{pk}) = (I_1 + \frac{2\lambda_0}{L_m})e^{-\frac{R(t_{pk}-t_7)}{L_s}} + \frac{V_m R\left[\sin(\omega t_{pk}) - \sin(\omega t_7)e^{-\frac{R(t_{pk}-t_7)}{L_s}}\right] + V_m\omega L_s\left[\cos(\omega t_7)e^{-\frac{R(t_{pk}-t_7)}{L_s}} - \cos(\omega t_{pk})\right]}{R^2 + (\omega L_s)^2} \tag{27}$$

$$V_m\sin(\omega t_{pk}) - R(I_1 + \frac{2\lambda_0}{L_m})e^{-\frac{R(t_{pk}-t_7)}{L_s}} - \frac{V_m R^2\left[\sin(\omega t_{pk}) - \sin(\omega t_7)e^{-\frac{R(t_{pk}-t_7)}{L_s}}\right] + V_m R\omega L_s\left[\cos(\omega t_7)e^{-\frac{R(t_{pk}-t_7)}{L_s}} - \cos(\omega t_{pk})\right]}{R^2 + (\omega L_s)^2} = 0 \tag{28}$$

$$t_7 = \frac{\arccos\left[\frac{V_m + \omega\left[(I_1 L_m + \lambda_0)e^{-\frac{R\left(\frac{T}{2} + \frac{L_s}{R}\ln\left(1 + \frac{\lambda_s - \lambda_3}{L_s I_3}\right)\right)}{L_m}} - \lambda_s\right]}{V_m}\right]}{\omega} \tag{29}$$

This article has been accepted for publication in a future issue of this journal, but has not been fully edited. Content may change prior to final publication. Citation information: DOI 10.1109/TPWRD.2015.2443560, IEEE Transactions on Power Delivery



$$B = K_1\left[\omega\cos\left(\frac{\omega T}{4}\right)+\frac{\omega^2 T}{4}\sin\left(\frac{\omega T}{4}\right)\right]-K_2 e^{-\frac{RT}{4L_s}}\left[\frac{R}{L_s}+\frac{R^2T}{4L_s^2}\right] - K_3\left[\omega\sin\left(\frac{\omega T}{4}\right)-\frac{\omega^2 T}{4}\cos\left(\frac{\omega T}{4}\right)\right]$$

$$C = K_3\left[\frac{\omega T}{4}\sin\left(\frac{\omega T}{4}\right)+\left(1-\frac{\omega^2T^2}{32}\right)\cos\left(\frac{\omega T}{4}\right)\right] - K_1\left[\frac{\omega T}{4}\cos\left(\frac{\omega T}{4}\right)+\left(\frac{\omega^2T^2}{32}-1\right)\sin\left(\frac{\omega T}{4}\right)\right] + K_2 e^{-\frac{RT}{4L_s}}\left[1+\frac{RT}{4L_s}+\frac{R^2T^2}{32L_s^2}\right] \quad (33)$$

with:

$$K_1 = V_m\omega^2 L_s^2$$
$$K_2 = e^{\frac{Rt_1}{L_s}}\left[-RI_1(R^2+\omega^2L_s^2)+V_mR^2\sin(\omega t_1) - V_mR\omega L_s\cos(\omega t_1)\right] \quad (34)$$
$$K_3 = V_mR\omega L_s$$

The linear and quadratic approximations of (28) are similar to (30) and (32). The only difference is parameter $K_2$:

$$K_2 = e^{\frac{Rt_7}{L_s}}\left[-R\left(I_1+\frac{2\lambda_0}{L_m}\right)(R^2+\omega^2L_s^2)+V_mR^2\sin(\omega t_7) - V_mR\omega L_s\cos(\omega t_7)\right] \quad (35)$$

Note that, the absolute value of $t_{pk}$ from (30) and (32) is used for the calculation of $i(t_{pk})$.

## V. Case Studies and Calculation Results

Two transformers (T1, T2) are selected to validate the calculations; T1 is a 1 kVA, four winding, standard, shell-type transformer and T2 is a 1 kVA, toroidal type transformer.

Currently, there are two basic arrangements for the iron-cores used to build distribution transformers: (1) in the shell-type, a continuously wound core is cut and wrapped around the windings a few laminations at a time; (2) in the core-type, cores are assembled by stacking laminations and the transformer is completed by sliding pre-made coils. As a consequence, both arrangements of the finished core are left with undesired air pockets between two stacked lamination pieces.

An alternative construction, not yet very common, is to use a core made of a continuous steel strip that is wound into a doughnut shape (toroid) and then wrapped entirely in coils. Therefore, for a toroidal geometry the core has a gapless construction with extremely low no-load losses. We are working to produce a distribution utility-grade toroidal core transformer [30]-[32]. The special construction of toroidal transformers leads to sharp and narrow hysteresis curve. Therefore, the residual flux after disconnection from the source is usually higher when compared to standard transformers. Also, the slopes of the magnetizing curve below the knee point and in deep saturation are different from the standard transformer. Because as we discussed, the standard transformer iron core has air pockets with equivalent linear reluctances that are along the flux path.

The difference is illustrated by comparison of two types of transformer hysteresis cycles in Fig. 1. The flat hysteresis cycle usually results in higher residual flux $\lambda_0$ after disconnection of the transformer from the source.

The worst cases of inrush and phase-hop currents happen when the transformer has residual flux. Reversible transient models [17], [18] are developed and used as the reference for validation of the calculated results. The transient models are first tested and validated with the comparison of the inrush and phase-hop currents versus laboratory measurements when the core is demagnetized (see Tables I and II). The results presented in Tables I and II show that the transient simulations (using the EMTP) are reliable for further studies.

TABLE I
First Peak of Inrush Current: Measurements Versus Transient (EMTP) Simulations For the Demagnetized Core

| | Winding | Measurements | Simulations | Difference (%) |
|---|---|---|---|---|
| $T_1$ | 1 | 157.7 | 162.5 | 3.04 |
| | 2 | 130.4 | 134.5 | 3.14 |
| | 3 | 125.2 | 122.3 | -2.32 |
| | 4 | 123.1 | 111.1 | -9.75 |
| $T_2$ | 1 | 325.0 | 334.9 | 3.04 |

TABLE II
Phase-Hop: Measurements Versus Transient (EMTP) Simulations For the Demagnetized Core

| | Winding | Measurements | Simulations | Difference (%) |
|---|---|---|---|---|
| $T_1$ | 1 | 328.9 | 330.2 | 0.39 |
| | 2 | 291.3 | 272.4 | -6.48 |
| | 3 | 261.7 | 252.5 | -3.51 |
| | 4 | 240.5 | 238.4 | -0.87 |
| $T_2$ | 1 | 490.0 | 481.9 | -1.6 |

The worst case of inrush currents is computed and compared versus simulations and the equations from references [9]-[11]. All parameter values such as initial flux are considered similar for the analytical methods and computer simulations in order to have a fair comparison. Table III presents the first peak of inrush current. In this table, the peak time $t_{pk}$ is calculated with three different methods; the exact (11), linear approximation (30), and quadratic approximation (32) formulas. The relative errors indicate that the analytical approach results of this paper are superior to the methods of [9]-[11]. However, the errors of the linear approximation formula (second order Taylor expansion) are not acceptable. Thus, the quadratic approximation (32) is recommended for the calculation of the first peak.

Methods of the references [9]-[11] show differences higher than 30% for some of the windings of the standard type transformers. Additionally, these methods have higher errors for toroidal transformers. The reason is that in the aforementioned methods the incremental flux is calculated with the integration of the terminal voltage rather than the internal voltage (*emf*). Therefore, the peak time ($t_{pk}$) which is the crucial factor for the calculation of the peak of inrush current is not estimated precisely.

The methods of [9]-[11] are suitable for large power transformers (transmission system level) that have small winding resistance. However, they may show errors for medium-size (distribution system level), or small-size transformers.

Table IV presents the calculation results for the phase-hop

This article has been accepted for publication in a future issue of this journal, but has not been fully edited. Content may change prior to final publication. Citation information: DOI 10.1109/TPWRD.2015.2443560, IEEE Transactions on Power Delivery



current. The analytical solutions of this paper are compared with EMTP simulations. The peak time $t_{pk}$ is obtained by the three formulae; the exact (11), linear approximation (30), and quadratic approximation (32). One can observe a very good agreement between all three methods and EMTP simulations with relative errors near 5%. The phase-hop current peak happens at the vicinity of the voltage wave peak (see Fig. 3(a)). Thus, the linear approximation is accurate enough for phase-hop current calculations.

It is worth mentioning that up until now there is no other method for the calculation of the phase-hop currents for comparison purposes. The analytical formulas for this transient current are presented in this paper for the first time.

Simulation and calculation results show that the first peak of inrush is more sensitive to the residual flux, while the phase-hop current does not change significantly when the iron core has residual flux.

A parametric study is carried out to evaluate the impact of the source impedance on the estimation of the maximum inrush currents. The source impedance is varied from 0.01 pu to 0.1 pu for $X/R$ ratios of 1, 5, 10, and 100. The calculation results are presented in Fig 6. Results show that the peak of inrush current is very sensitive to the source impedance. However, the relative ratio of the reactance and resistance of the source does not affect the results.

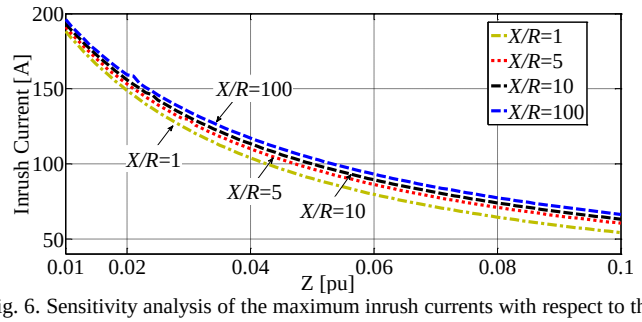


Fig. 6. Sensitivity analysis of the maximum inrush currents with respect to the source impedance variations.

## VI. Numerical Example

In this section, the calculation results for the inrush and phase-hop currents for the second winding of T1 are presented. The required data is presented in Table V. For this example, measurements are carried out in a low voltage laboratory and therefore, the short circuit inductance ($L_{sc}$) is negligible. The total resistance is $R=R_{sc}+R_T=0.1+0.443=0.543\ \Omega$.

The objective is to calculate the first and second peaks of inrush current with (10) and (27), respectively. For this, parameter $t_{pk}$ needs to be obtained from (32) or (30). Equation (30) is accurate enough to calculate $t_{pk}$ for the second peak (phase-hop current). However, (32) needs to be used to calculate $t_{pk}$ for the first peak of inrush current.

From (31), (33), (34) and (35) one can observe that the parameters $K$, $A$, $B$, and $C$ are functions of $R$, $\omega$, $L_s$, $T$, $V_m$, $\lambda_0$, $L_m$, $t_1$, $I_1$, and $t_7$. Parameters $R$, $\omega$, $L_s$, $T$, $V_m$, $\lambda_0$, $L_m$ are known, and $t_1$, $I_1$, and $t_7$ can be calculated with (6), (7), and (29), respectively. Also, $t_7$, $I_3$ and $\lambda_3$ are retained from (12) and (13), respectively. Having these parameters, the next step is to calculate $K_1$, $K_2$, and $K_3$:

1) To calculate the first peak, $K_1$, $K_2$, and $K_3$ should be determined from (34). Then, these three parameters are substituted into (33) to get $A$, $B$, and $C$ required for solving the quadratic equation (32).
2) To calculate the second peak (phase-hop), $K_1$ and $K_3$ are calculated from (34), and $K_2$ is calculated from (35). Then, these three parameters are substituted into (31) to get $A$ and $B$ required for solving the linear equation (30).

The step by step calculations including the corresponding formulae are summarized in Tables VI and VII. The calculation of the first peak of inrush and the phase-hop currents require 10 and 12 individual steps, respectively. One can observe that the calculation of the parameters in several steps is simple and straight forward.

## VII. Conclusions

An enhanced method for the calculation of the maximum inrush currents of power transformers during the energization was proposed. First, the method was applied to compute the inrush currents caused by zero crossing switching with maximum residual flux in the iron core (worst case scenario). Then, the method was extended to the calculation of phase-hop currents. The calculations for both inrush and phase-hop currents

TABLE III
Highest Peak of Inrush Current: Calculations Versus EMTP Simulations and Other Methods

| Winding | | Simulations (Reference) | [9], [11] | Diff. (%) | [10] | Diff. (%) | Analytical Exact (11) | Diff. (%) | Analytical Appr. (30) | Diff. (%) | Analytical Appr. (32) | Diff. (%) |
|---|---|---|---|---|---|---|---|---|---|---|---|---|
| T1 | 1 | 201.7 | 256.5 | 27.2 | 546.1 | 170.7 | 218.2 | 8.2 | 147.1 | -27.1 | 194.6 | -3.5 |
| | 2 | 168.9 | 210.6 | 24.7 | 414.4 | 145.3 | 175.9 | 4.1 | 129.7 | -19.4 | 167.6 | -0.8 |
| | 3 | 155.8 | 193.2 | 24.0 | 329.5 | 111.4 | 156.3 | 0.3 | 132.6 | -11.5 | 151.6 | -2.1 |
| | 4 | 142.2 | 178.4 | 25.5 | 271.0 | 90.5 | 141.2 | -0.7 | 131.8 | -5.2 | 138.0 | -2.1 |
| T2 | 1 | 475.1 | 829.1 | 74.5 | 2627.0 | 452.9 | 477.6 | 0.5 | 477.4 | 1.1 | 477.6 | 1.2 |

TABLE IV
Worst Case of Phase-Hop: Calculations Versus EMTP Simulations

| Winding | | Simulations (Reference) | Analytical Exact (28) | Diff. (%) | Analytical Appr. (30) | Diff. (%) | Analytical Appr. (32) | Diff. (%) |
|---|---|---|---|---|---|---|---|---|
| $T_1$ | 1 | 330.5 | 350.1 | 5.9 | 349.6 | 5.8 | 350.1 | 5.9 |
| | 2 | 272.8 | 288.7 | 5.8 | 287.9 | 5.5 | 288.7 | 5.8 |
| | 3 | 253.1 | 268.5 | 6.0 | 266.6 | 5.3 | 268.5 | 6.0 |
| | 4 | 239.4 | 253.0 | 5.7 | 248.7 | 3.9 | 253.1 | 5.7 |
| $T_2$ | 1 | 481.9 | 485.3 | 0.7 | 485.3 | 0.7 | 485.3 | 0.7 |

This article has been accepted for publication in a future issue of this journal, but has not been fully edited. Content may change prior to final publication. Citation information: DOI 10.1109/TPWRD.2015.2443560, IEEE Transactions on Power Delivery



were compared with the transient simulations, laboratory measurements, and three widely-used formulas. Results indicate that the method of this paper is more accurate than the previously published formulas.

The method presented in the paper is simple to use by engineers in the field to estimate the maximum possible inrush currents with high accuracy without using circuit simulation programs. The method can be easily implemented in the design programs since it is suitable for spread sheets and even calculators.

This paper only deals with single-phase transformers. It is believed that the same analytical method could be applied to a duality derived equivalent circuit for large three-phase transformers. Analytical formulae to calculate the maximum inrush and phase-hop currents for three-phase transformers would be presented in an upcoming paper.

TABLE V
DATA FOR THE SECOND WINDING OF T1

| $V_m$ [V] | $R$ [Ω] | $L_m$ [H] | $L_s$ [H] | $\lambda_0$ [Wb.] | $\lambda_s$ [Wb.] | $I_0$ [A] | $f$ [Hz] |
|---|---|---|---|---|---|---|---|
| 179.5 | 0.543 | 0.411 | 0.00085 | 0.1 | 0.7 | 0.1 | 60 |

## VIII. REFERENCES


[1] T. R. Specht, "Transformer Magnetizing Inrush Currents," *AIEE Transactions*, vol. 70, no. 4, pp. 324, Apr. 1951.

[2] L. F. Blume. *Transformer Engineering*, John Wiley and Sons, Inc., New York, N. Y., 1938, pp. 23-26.

[3] A. B. Knowlton, *Standard Handbook for Electrical Engineers*, McGraw-Hill Book Company, Inc., New York, N. Y., seventh edition, Aug. 1941, p. 52.

[4] *Electrical Transmission and Distribution Reference Book*, 3rd ed. East Pittsburgh, PA: Westinghouse Electric and Manufacturing Company, 1944, pp. 411–416.

[5] W. K. Sonneman, C. L. Wagner, and G. D. Rockefeller, "Magnetizing inrush phenomena in transformer banks," *IEEE Trans. Power App. Syst.*, vol. 77, pp. 884-892, Oct. 1958.

[6] J. E. Holcomb, "Distribution Transformer Magnetizing Inrush Current," *AIEE Transactions*, vol. 80, no. 3, pp. 697-702, Apr. 1961.

[7] T. R. Specht, "Transformer Inrush and Rectifier Transient Currents," *IEEE Trans. Power App. Syst.*, vol. PAS-88, no. 4, pp. 269-276, Apr. 1969.

[8] R. Yacamini and A. Abu-Nasser, "Numerical calculation of inrush current in single-phase transformers", *1EE Proc.*, vol. 128, Pt. B, no. 6, pp. 327-334, Nov. 1981.

[9] R. S. Girgis and E. G. teNyenhuis, "Characteristics of Inrush Current of Present Designs of Power Transformers," in *proc. IEEE Power Eng, Soc. General Meeting*, pp. 1-6, Jun. 2007.

[10] S. E. Zirka, Y. I. Moroz, C. M. Arturi, N. Chiesa, and H. K. Høidalen, "Topology-Correct Reversible Transformer Model," *IEEE Trans. Power Del.*, vol. 27, no. 4, pp. 2037–2045, Oct. 2012.

[11] Y. Wang, S. G. Abdulsalam, and W. Xu, "Analytical Formula to Estimate the Maximum Inrush Current," *IEEE Trans. Power Del.*, vol. 23, no. 2, pp. 1266–1268, Apr. 2008.

[12] W. K. Macfayden, R. R. S. Simpson, R. D. Slater, and W. S. Wood, "Method of predicting transient-current patterns in transformers," *IEE Proc.*, vol. 120, no. 11, pp. 1393-1396, Nov. 1973.

[13] J. W. Teape, R. D. Slater, R. R. S. Simpson, and W.S. Wood, "Hysteresis effects in transformers, including ferroresonance," *IEE Proc.*, vol. 123, no. 2, pp. 153-158, Feb. 1976.

[14] H. L. Nakra and T.H. Barton, "Three-phase transformer transients," *IEEE Trans. Power App. Syst.*, vol. PAS-93, no. 6, pp. 1810-1819, Nov. 1974.

[15] R. Yacamini and A. Abu-Nasser, "The calculation of inrush current in three-phase transformers," *1EE Proc.*, vol. 133, Pt. B, no. 1, pp. 31-40, Jan. 1986.

[16] R. Yacamini and H. Bronzeado, "Transformer inrush calculations using a coupled electromagnetic model," *IEE Proc.-Sci. Mens. Technol.*, vol. 141, no. 6, pp. 491-495, Nov. 1994.

[17] S. Jazebi, F. de León, A. Farazamand, and D. Deswal, "Dual Reversible Transformer Model for the Calculation of Low-Frequency Transients", *IEEE Trans. Power Del*., vol. 28, pp. 2509-2517, Oct. 2013.

[18] S. Jazebi and F. de León, "Experimentally Validated Reversible Single-Phase Multi-Winding Transformer Model for the Accurate Calculation of Low-Frequency Transients," *IEEE Trans. Power Del.*, vol. 30, pp. 193-201, Feb. 2015.

[19] E. Styvaktakis, M. H. J. Bollen, and I. Y. H. Gu, "Transformer saturation after a voltage dip," *IEEE Power Eng. Rev.* vol. 20, pp. 62–64, Apr. 2000.

[20] L. Guasch, F. Córcoles, J. Pedra, and L. Sáinz, "Effects of Symmetrical Voltage Sags on Three-Phase Three-Legged Transformers," *IEEE Trans. Power Del.*, vol. 19, pp. 875-883, Apr. 2004.

[21] L. Sáinz, F. Córcoles, J. Pedra, and L. Guasch, "Theoretical Calculation of Inrush Currents in Three- and Five-Legged Core Transformers," *IEEE Trans. Power Del.*, vol. 22, pp. 986-995, Apr. 2007.

[22] A. S. Masoum, P. S. Moses, and A. Abu-Siada, "Impact of Voltage Sags on Three-Phase Power Transformers," in *Proc. 2010Universities Power Engineering Conf.*, pp. 1-6.

[23] H. Xie, L. Ängquist, and H. Nee, "Comparison of Voltage and Flux Modulation Schemes of StatComs Regarding Transformer Saturation During Fault Recovery," *IEEE Trans. Power Syst.*, vol. 23, pp. 1653-1661, Nov. 2008.

[24] A. Farazmand, F. de León, K. Zhang, and S. Jazebi, "Analysis, Modeling and Simulation of the Phase-Hop Condition in Transformers: The Largest Inrush Currents," *IEEE Trans. Power Del.*, vol. 29, pp. 1918-1926, Aug. 2014.

[25] Slow Transients Task Force of the IEEE. Modeling and Analysis of System Transients Using Digital Programs Working Group "Modeling and Analysis Guidelines for Slow Transients--Part III: The Study of Ferroresonance," *IEEE Trans. Power Del.*, vol. 15, pp. 255–265, Jan. 2000.

[26] H. L. Willis and M. H. Rashid, *Protective Relaying Principles and Applications*, Taylor & Francis Group LLC., Third Edition, 2006.

[27] *IEEE Standard Test Code for Dry-Type Distribution and Power Transformers, Recognized as an American National Standard (ANSI)*, IEEE Standard C57.12.91-1995, 1995.

[28] F. de León, S. Jazebi, and A. Farazmand, "Accurate measurement of the air-core inductance of iron-core transformers with a non-ideal low power rectifier," *IEEE Trans. Power Del*., vol. 29, pp. 294-296, Feb. 2014.

[29] R. Doğan, S. Jazebi, and F. de León, "Investigation of Transformer-Based Solutions for the Reduction of Inrush and Phase-Hop Currents," submitted to *IEEE Trans. on Power Elect.*, Jun. 2015.

[30] P. Gómez, F. de León, and I. Hernández, "Impulse Response Analysis of Toroidal Core Distribution Transformers for Dielectric Design," *IEEE Trans. Power Del*., vol. 26, pp. 1231-1238, Apr. 2011.

[31] S. Purushothaman and F. de León, "Heat Transfer Model for Toroidal Transformers," *IEEE Trans. Power Del*., vol. 27, pp. 813-820, Apr. 2012.

[32] I. Hernández, F. de León, and P. Gómez, "Design Formulas for the Leakage Inductance of Toroidal Distribution Transformers," *IEEE Trans. Power Del*., vol. 26, pp. 2197-2204, Oct. 2011.

[33] F. de León, "Electrostatic Shielding of Transformers," U.S. Patent 14/338048, Jan. 29, 2015.


TABLE VI
STEP BY STEP CALCULATIONS OF THE FIRST PEAK OF INRUSH

| Step | 1 | 2 | 3 | 4 | 5 | 6 | 7 | 8 | 9 | 10 |
|---|---|---|---|---|---|---|---|---|---|---|
| Parameter | $t_1$ [ms] | $I_1$ [A] | $K_1$ | $K_2$ | $K_3$ | $A$ | $B$ | $C$ | $t_{pk}$ [ms] | $i(t_{pk})$ [A] |
| Equation | (6) | (7) | (34) | (34) | (34) | (33) | (33) | (33) | (32) | (10) |
| Inrush | 4.86 | 1.46 | 18.4 | 1,317.9 | 31.2 | 17,466,901 | -216,117 | 707.6 | 6.4 | 167.6 |

TABLE VII
STEP BY STEP CALCULATIONS OF THE PHASE-HOP CURRENT

| Step | 1 | 2 | 3 | 4 | 5 | 6 | 7 | 8 | 9 | 10 | 11 | 12 |
|---|---|---|---|---|---|---|---|---|---|---|---|---|
| Parameter | $t_1$ [ms] | $I_1$ [A] | $I_3$ [A] | $\lambda_3$ [Wb] | $t_7$ [ms] | $K_1$ | $K_2$ | $K_3$ | $A$ | $B$ | $t_{pk}$ [ms] | $i(t_{pk})$ [A] |
| Equation | (6) | (7) | (12) | (13) | (29) | (34) | (35) | (34) | (31) | (31) | (30) | (27) |
| Phase-Hop | 4.86 | 1.46 | 114.9 | 0.796 | 0.24 | 18.4 | -31.1 | 31.2 | -10,385 | 59.5 | 5.73 | 287.9 |